

Joint probability analysis of storm surge and wave caused by tropical cyclone for the estimation of protection standard: a case study on the eastern coast of the Leizhou Peninsula and Hainan Island of China

Zhang Haixia^{1,2,3,4}, Cheng Meng^{1,2,3,4}, Fang Weihua^{1,2,3,4}

5 ¹Key Laboratory of Environmental Change and Natural Disasters, Ministry of Education, Beijing Normal University, 100875, Beijing, China

²Academy of Disaster Risk Science, Faculty of Geographical Science, Beijing Normal University, 100875, Beijing, China

³Southern Marine Science and Engineering Guangdong Laboratory (Guangzhou), 511458, Guangzhou, Guangdong, China

10 ⁴State Key Laboratory of Earth Surface Processes and Resource Ecology (ESPRE), Beijing Normal University, 100875, Beijing, China

Correspondence to: Weihua Fang (weihua.fang@bnu.edu.cn)

Abstract. The impact of natural hazards such as storm surges and waves on coastal areas during extreme tropical storm events can be amplified by the cascading effects of multiple hazards. Quantitative estimation of the marginal distribution and joint probability distribution of storm surge and wave is essential to understanding and managing tropical cyclone disaster risks. In this study, the dependence between storm surges and waves is quantitatively assessed using the extreme value theory and copula function for the Leizhou Peninsula and Hainan Island of China, based on the numerically simulated surge height (SH) and significant wave heights (SWH) for every 30 minutes from 1949 to 2013. The steps for determining coastal protection standards in scalar values are also demonstrated. It is found that, first, the generalized extreme value (GEV) function and Gumbel copula function are suitable, respectively, for fitting the marginal and joint distribution characteristics of the SHs and SWHs in this study area. Additionally, SH shows higher values as locations get closer to the coastline, and SWH becomes higher further from the coastline. Lastly, the optimal design criteria of SH and SWH under different joint return periods can be estimated using the non-linear programming method. This study shows the effectiveness of the bivariate copula function in evaluating the probability for different scenarios, providing a valuable reference for optimizing engineering design criteria.

25 **Keywords:** Joint probability analysis, Storm surge and wave, Copula function, Tropical cyclone, Leizhou Peninsula and Hainan Island

1 Introduction

Tropical cyclone storm surges and waves could cause severe loss of life and property in offshore and coastal areas (Chen and Yu, 2017; Marcos et al., 2019; Wahl et al., 2015), and it is of great importance to quantify the intensity-frequency relationship of storm surges and waves, to understand the joint severity of multi-hazard extreme tropical cyclones (Zhang and Wang, 2021; Galiatsatou and Prinos, 2016).

In the past, many studies have analyzed the single hazard indicators for tropical cyclone storm surges and waves (Lin et al., 2010; Shi et al., 2020; Teena et al., 2012), often with observed time series data, or with or simulated results by numerical models (Petroliagkis et al., 2016; Bilskie1 et al., 2016; Huang et al., 2013; Papadimitriou et al., 2020). The intensity values of the surge height (SH) or significant wave height (SWH) of a specific return period can be estimated based on extreme value theory (Teena et al., 2012; Muraleedharan et al., 2007; Morellato and Benoit, 2010; Niedoroda et al., 2010). Accordingly, the estimated probabilities of single hazards, such as SH or SWH, have also been widely applied in the protection standard design in coastal areas (Bomers et al., 2019; Perk et al., 2019; Lee and Jun, 2006).

However, strong storm surges and waves often occur simultaneously during tropical cyclone events, which often cause greater impact than estimated only by a single variate due to the cascading effects of multi-hazards. For example, when high waves near the coast take place along strong storm surges, the overtopping and overflowing at sea dyke can lead to a large area of inundation and severe damage to coastal facilities (Rao et al., 2012; Hughes and Nadal, 2009; Pan et al., 2019). Similarly, rising sea levels due to storm surges would improve the probability of wave overtopping (Pan et al., 2013; Li et al., 2012). The concurrent interaction between storm surges and waves often assesses the effects of multi-hazards with significant uncertainties. Some studies have investigated the physical interaction of storm surges and waves through numerical simulation by coupling storm surge and wave models (Xie et al., 2016; Kimf et al., 2016; Brown, 2010) for specific events.

Statistical tools such as joint probability analysis have been used in multidimensional natural hazard assessment (Hsu et al., 2018). Since the Copula function does not restrict the marginal distribution function and can be relatively easily extended to multiple dimensions, it is often used to construct joint probability of multiple variates (Nelsen, 2006; Chen and Guo, 2019). There are a variety of applications with Copula function for double hazards, for example, rainfall and storm surge (Jang and Chang, 2022), wind and storm surge (Trepanier et al., 2015), and storm surge and wave (Corbella and Stretch, 2013; Wahl et

al., 2012).

In coastal protection standard design, it is essential to analyze and estimate the joint probability of SH and SWH. Chen et al. (2019) used the copula functions to analyze the joint probability of extreme wave height and surge height at nine representative stations along China's coasts. Galiatsatou and Prinos (2016) investigated the joint probability of extreme wave heights and storm surges with time by a non-stationary bivariate approach. Marcos et al. (2019) statistically assessed the dependence between extreme storm surges and wind waves along global coastal areas using the outputs of numerical models. Most previous joint probability studies on storm surges and waves mainly focused on location-specific rather than region-wide analysis. In addition, even with the joint probability of bivariate estimation, only an intercepted curve can be obtained since their probability is a three-dimensional surface. It is not applicable for actual protection design without a specific scalar value for SH or SWH.

In this study, we aim to explore the joint probability characteristics of tropical cyclone storm surges and waves for large coastal areas and to investigate the methods and steps for selecting the protection standard of sea dikes. Firstly, we fit the marginal and copula function of nodes in the study area based on the numerically simulated tropical cyclone SH and SWH from 1949 to 2013. Next, the optimal functions are selected for every modeling node based on the Kolmogorov-Smirnov (K-S) test, AIC, and BIC. Then, the correlation between SH and SWH is quantified using the copula function to calculate the probabilities under simultaneous, joint, conditional, and different-level combinations. Finally, the bivariate probability changes caused by increasing SH and SWH are quantitatively assessed, and the design storm surges and waves for different joint return periods are estimated based on a non-linear programming method.

2 Study area and data

2.1 Best tracks of TCs

The best track dataset of historical TCs in the Northwest Pacific (NWP) is obtained from the Tropical Cyclone Data Center of the China Meteorological Administration (CMA). The CMA records in detail the location (longitude and latitude), time (year, month, day, hour), central minimum pressure, and 2-minute average near-center maximum sustained wind speed (MSW) for

every 6-hour track point of each TC event since 1949 (Lu et al., 2021). The landfall of TCs in China is concentrated on the
75 southeast coast, especially in the coastal areas of the South China Sea. Figure 1a shows the spatial distribution of the best track
and maximum sustained wind speed of 86 historical TCs screened in this study from 1949 to 2013.

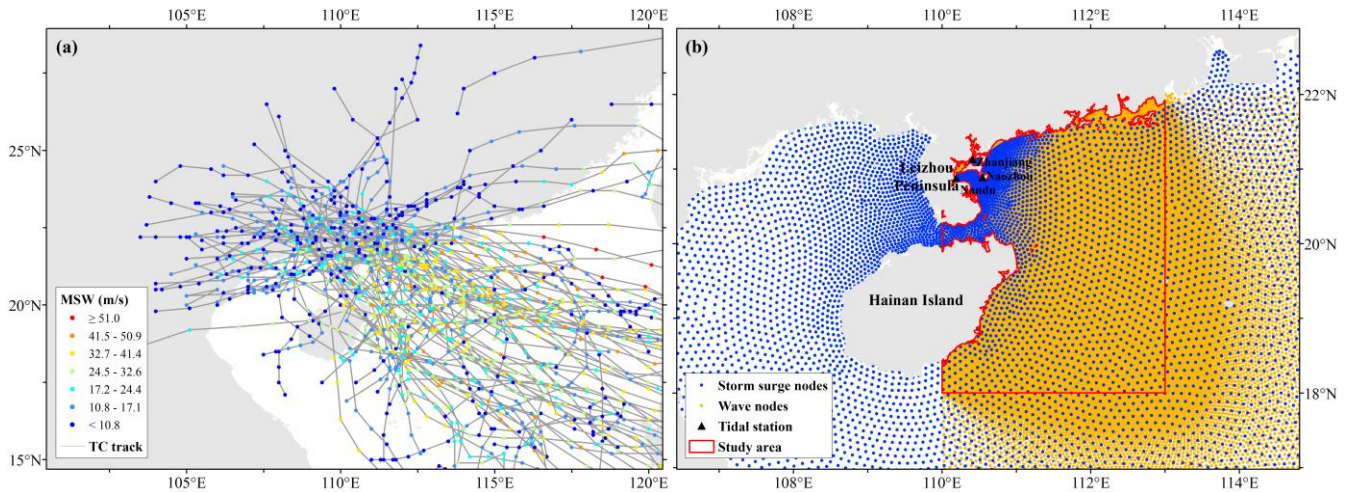


Figure 1: Best track and MSW of 86 TCs in this study from 1949 to 2013 (a) and the study area for the joint probability analysis of storm surges and waves of TCs (b).

80 2.2 Surge heights

The TC surge heights (SHs) dataset is obtained from the Ocean University of China, mainly through the ADvanced CIRCulation model (ADCIRC) simulations, which includes the SHs of 86 TCs affecting the eastern coast of the Leizhou Peninsula and Hainan Island from 1949 to 2013 (Liu et al., 2018; Li et al., 2016). The previous study provides a water depth map for the study area (Liu et al., 2018). The ADCIRC model integrates the effects of various boundary conditions and external
85 forcing and uses triangular grids with different resolutions, making it more computationally efficient and applicable in numerical simulations. The simulation results are the total water level after the superposition of the water gain caused by a tropical cyclone and astronomical tide, and the time step is 30 minutes. To improve the simulation accuracy and computing speed of the hot spot area, the model adopts a triangular grid with nested small- and large-area grids, and the resolutions of different area grids are set in a gradual resolution range from 0.0039° to 0.3°. Comparing the simulation values with the
90 measured surge height at the observation sites, we discover that the absolute standard error is 47 cm, the relative standard error is 22%, and the simulation results are similar to the observed values in most cases. Thus, the dataset could be used to assess

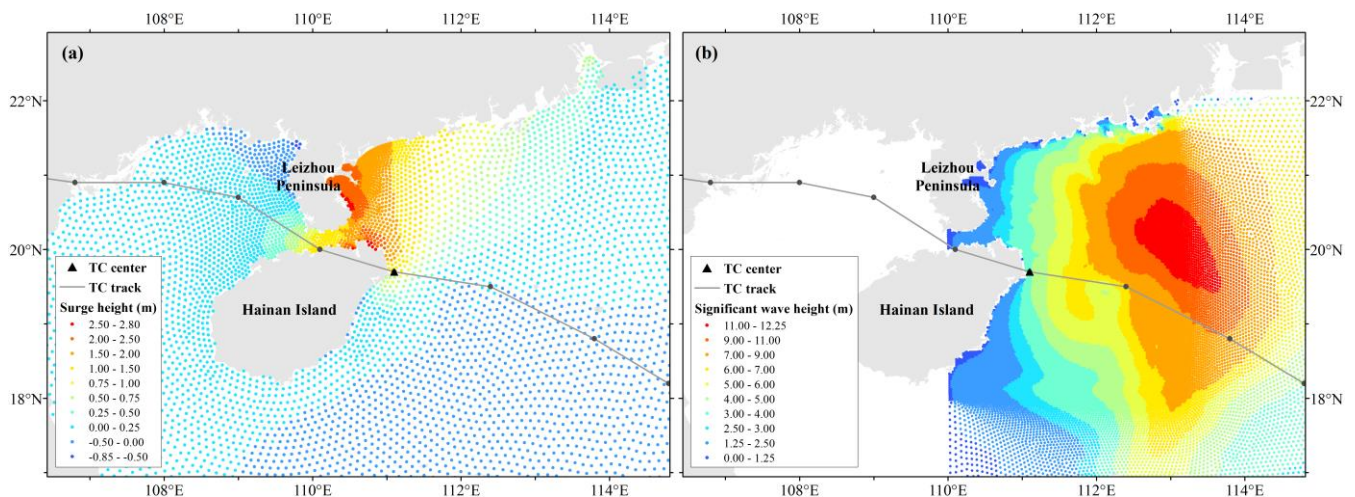
the hazard of TC storm surges. Figure 2a shows an example of the simulation results of the surge height of TC *Nasha* (ID:1117) at a specific moment.

2.3 Significant wave heights

95 The TC significant wave heights (SWHs) dataset is also obtained from the Ocean University of China, mainly through the Simulating WAVes Nearshore (SWAN) model, and includes the SWHs of 86 TC events affecting the study area from 1949 to 2013 (Li et al., 2016). The SWAN model has the advantage of high computational accuracy and stability and has been widely used in numerical simulations of offshore waters. The simulation results include indicators such as significant wave height, mean period, and wave direction, and the time step is 1 hour. The model also uses a triangular grid with nested small- and large-area grids and gradual resolution, but the nodes' scopes and locations differ from those of the storm surge model.

100 Comparing the observed data of buoy stations with the simulated values reveals that the unstructured grid can well reflect the wave variation conditions in the sea. In addition, the mean absolute and root mean square errors of the simulated results of the locally encrypted unstructured triangular grid are the smallest, indicating that the data can effectively reproduce the wave distribution during tropical cyclones. It shall be noted that the effect of sea level rise due to storm surge was not considered

105 during the SWH simulation, which will influence the accuracy of SWHs, especially in intermedia and shallow water. In this paper, we choose the SWH as an indicator of tropical cyclone wave hazard. Figure 2b shows an example of the significant wave height of TC *Nasha* (ID: 1170) at a specific moment.



110 **Figure 2: Distribution of surge height (a) and significant wave height (b) at a specific moment of TC *Nasha* (ID: 1117) (UTC: 2011.9.29 6:00:00)**

2.4 Study area

Based on the location of the nodes of the triangular grid in the storm surge (Section 2.2) and wave datasets (Section 2.3), we select the region with a dense distribution of both as the study area, and the finalized spatial range is 110°E - 113°E, 18°N - 22°N (Figure 1b). This area is located east of the Leizhou Peninsula and Hainan Island in the South China Sea, which is one of the most frequently affected areas by tropical cyclones in China. Based on the dataset of surge height (SH) and significant wave height (SWH) of tropical cyclones, we screen 86 historical tropical cyclones (TC) events that simultaneously affected the study area from 1949 to 2013 for joint probability characteristics analysis of storm surge and wave.

3 Methods

120 Sklar (Sklar, 1973) elucidates the role that copula play in the relationship between multivariate distribution and their univariate margins distribution, and states that any multivariate joint distribution can be described by a univariate marginal distribution function and a couple describing the dependence structure between the variables (Nelsen, 2006). Let $F(x)$ and $G(y)$ be the marginal distributions of x and y , C is the copula, and $H(x,y) = C(F(x),G(y))$, where H is the bivariate joint distribution function of x and y (Serinaldi, 2015). Therefore, the copula function is widely utilized in multi-hazard joint probability analysis of natural disasters (Chen et al., 2019; Lee et al., 2013).

125 3.1 Marginal function

The marginal function means that the probability density function (PDF) and cumulative distribution function (CDF) of the univariate are constructed by intensity-frequency analysis to reflect the probability of occurrence of the univariate at different intensities. The method is widely utilized in natural hazard assessments such as tropical cyclones, floods, droughts, and earthquakes. We select five commonly employed marginal functions for the annual extreme values fitting of tropical cyclone storm surges and waves, including the Gumbel, Weibull, gamma, exponential, and generalized extreme value (GEV) functions. In this study, the maximum likelihood method is used to estimate the function parameters, based on which the optimal marginal

functions for SHs and SWHs are screened by the following steps: Firstly, the p-value of the K-S test is used to determine whether each node rejects the hypothesis that the samples obey a certain functional distribution. Secondly, the optimal function for each node is screened by the three metrics, AIC, BIC, and D-value of the K-S test. The smaller the AIC, BIC, and D-value of the K-S test, the better the goodness of fit, thus determining the optimal marginal function for each node. Finally, an optimal function is selected as the univariate marginal function for all nodes, and its PDF and CDF are fitted.

3.2 Bivariate copula function

There are a variety of copulas families, including Meta-elliptical copulas (normal and t), Archimedean copulas (Clayton, Gumbel, Frank, and Ali-Mikhail-Haq), Extreme Value copulas (Gumbel, Husler-Reiss, Galambos, Tawn, and t-EV), and the other families (Plackett and Farlie-Gumbel-Morgenstern) (Chen and Guo, 2019). Among these copulas, the Archimedean copula is more popular for hydrologic applications. The commonly employed Archimedean copula functions include Gumbel, Clayton, and Frank (Table 1), which are selected to analyze the joint probabilities of two variables, the SHs, and SWHs of a tropical cyclone. Then the maximum likelihood method is used to estimate the parameters of the copula function. Next, we fit the goodness-of-fit of copula functions for the tropical cyclone storm surge and waves at each node by the K-S test. According to the passing rate of the K-S test at the sample nodes, an optimal function is selected as the copula function for all nodes of the two-dimensional variables, and the PDF and CDF are calculated.

Table 1 Formulas and parameter ranges for three types of bivariate Archimedean copula functions.

Name of copula	Bivariate Copula	Parameter θ
Clayton	$C_{\theta}(u, v) = [\max \{u^{-\theta} + v^{-\theta} - 1; 0\}]^{-1/\theta}$	$\theta \in [-1, \infty) \setminus \{0\}$
Frank	$C_{\theta}(u, v) = -\frac{1}{\theta} \log \left[1 + \frac{(e^{-\theta u} - 1)(e^{-\theta v} - 1)}{e^{-\theta} - 1} \right]$	$\theta \in R \setminus \{0\}$
Gumbel	$C_{\theta}(u, v) = \exp \left[-\left((-\log(u))^{\theta} + (-\log(v))^{\theta} \right)^{\frac{1}{\theta}} \right]$	$\theta \in [1, \infty)$

Note: u and v are uniform (0,1) random variables (Nelsen, 2006).

3.3 Joint probability of storm surges and waves

150 3.3.1 Univariate return period

The return period (RP) indicates the period of natural hazard events, and it is a crucial indicator for quantifying the hazard level, which is widely utilized in hazard analysis. The formula for the return period of a single hazard indicator is as follows.

$$RP_X = \frac{E_L}{1 - F_X(x)} = \frac{E_L}{1 - P(X \leq x)} \quad (1)$$

where RP_X is the return period of the univariate X ; $F_X(x) = P(X \leq x)$ is the marginal function of the univariate X ; and E_L denotes the time interval of the sample series of the univariate X , the value is taken as 1 in this paper.

155 3.3.2 Bivariate probability and return period

Based on the copula function, it can quantitatively estimate the probability of a multivariate being greater than a specified threshold. The bivariate probability refers to the likelihood that various conditions will occur simultaneously, and the bivariate return period refers to the average time interval required for multiple states to be simultaneously greater than a certain threshold. The definitions of three types of joint probabilities and return periods are given according to the univariate return period formula. The first type is when two variables simultaneously reach a given threshold, which will be defined as the simultaneous probability P_\cap (Eq. 2) and simultaneous return period RP_\cap (Eq. 3). The second type is that at least one variable reaches a given threshold, which is defined as the joint probability P_\cup (Eq. 4) and joint return period RP_\cup (Eq. 5). The third type is the conditional probability P_1 (Eq. 6) and conditional return period RP_1 (Eq. 7), where when one of the variables reaches a given threshold, the other variable also reaches a certain threshold. The formula is as follows (Serinaldi, 2015):

$$\begin{aligned} P_\cap &= P((X > x) \cap (Y > y)) = 1 - P(X \leq x) - P(Y \leq y) + P(X \leq x, Y \leq y) \\ &= 1 - F_X(x) - F_Y(y) + F_{X,Y}(x, y) \end{aligned} \quad (2)$$

$$RP_\cap = \frac{E_L}{P((X > x) \cap (Y > y))} = \frac{E_L}{1 - F_X(x) - F_Y(y) + F_{X,Y}(x, y)} \quad (3)$$

$$P_\cup = P((X > x) \cup (Y > y)) = 1 - P(X \leq x, Y \leq y) = 1 - F_{X,Y}(x, y) \quad (4)$$

$$RP_\cup = \frac{E_L}{P((X > x) \cup (Y > y))} = \frac{E_L}{1 - F_{X,Y}(x, y)} \quad (5)$$

$$P_1 = P((X > x)|(Y > y)) = \frac{P(X > x, Y > y)}{P(Y > y)} = \frac{1 - P(X \leq x) - P(Y \leq y) + P(X \leq x, Y \leq y)}{1 - P(Y \leq y)} \quad (6)$$

$$= \frac{1 - F_X(x) - F_Y(y) + F_{X,Y}(x, y)}{1 - F_Y(y)}$$

$$RP_1 = \frac{E_L}{P((X > x)|(Y > y))} = \frac{E_L \cdot (1 - F_Y(y))}{1 - F_X(x) - F_Y(y) + F_{X,Y}(x, y)} \quad (7)$$

165 where $F_X(x)$ and $F_Y(y)$ are the marginal functions of the univariate X and Y , respectively, and $F_{X,Y}(x, y)$ is the joint distribution function of the two-dimensional variables (X, Y) .

3.3.3 Combined scenario probability

To carry out the tropical cyclone storm surge and wave combination scenario simulation, we classify the SH and SWH into five classes (Table 2) by referring to the *Technical directives for risk assessment and zoning of marine disasters—Part 1: Storm Surge* (MNR, 2019) and *Part 2: Waves* (MNR, 2021). We calculate the bivariate probabilities for discretized hazard level combination scenarios based on the marginal and copula functions of the storm surge and wave. The formula is as follows:

$$P_{\&} = P(x_1 < X \leq x_2, y_1 < Y \leq y_2)$$

$$= P(X \leq x_2, Y \leq y_2) - P(X \leq x_2, Y \leq y_1) - P(X \leq x_1, Y \leq y_2) + P(X \leq x_1, Y \leq y_1) \quad (8)$$

$$= F_{X,Y}(x_2, y_2) - F_{X,Y}(x_2, y_1) - F_{X,Y}(x_1, y_2) + F_{X,Y}(x_1, y_1)$$

Table 2 Hazard level classification criteria for combined scenarios of tropical cyclone surge height and significant wave height

Hazard level	Surge height (m)	Significant wave height (m)
I	[2.5, +∞)	[14.0, +∞)
II	[2.0, 2.5)	[9.0, 14.0)
III	[1.5, 2.0)	[6.0, 9.0)
IV	[1.0, 1.5)	[4.0, 6.0)
V	[0.0, 1.0)	[0.0, 4.0)

3.4 Design of protection standards for storm surge and wave

3.4.1 Probability changes under increased storm surge and wave protection standards

175 In actual engineering protection design, if the protection standards of SH and SWH are appropriately increased or decreased, it can change the simultaneous bivariate probability P_{\cap} , joint bivariate probability P_{\cup} , and conditional bivariate probability

P_1 . In this paper, we try to estimate the change value of the bivariate probability by raising the return period of storm surge or wave. The formula is as follows:

$$\begin{aligned}
P_{d\cap} &= P((X > x_2) \cap (Y > y)) - P((X > x_1) \cap (Y > y)) \\
&= P(X \leq x_2, Y \leq y) - P(X \leq x_2) - P(X \leq x_1, Y \leq y) + P(X \leq x_1) \\
&= F_{X,Y}(x_2, y) - F_X(x_2) - F_{X,Y}(x_1, y) + F_X(x_1)
\end{aligned} \tag{9}$$

$$\begin{aligned}
P_{d\cup} &= P((X > x_2) \cup (Y > y)) - P((X > x_1) \cup (Y > y)) = P(X \leq x_1, Y \leq y) - P(X \leq x_2, Y \leq y) \\
&= F_{X,Y}(x_1, y) - F_{X,Y}(x_2, y)
\end{aligned} \tag{10}$$

$$\begin{aligned}
P_{d|} &= P((X > x_2)|(Y > y)) - P((X > x_1)|(Y > y)) \\
&= \frac{P(X \leq x_2, Y \leq y) - P(X \leq x_2) - P(X \leq x_1, Y \leq y) + P(X \leq x_1)}{1 - P(Y \leq y)} \\
&= \frac{F_{X,Y}(x_2, y) - F_X(x_2) - F_{X,Y}(x_1, y) + F_X(x_1)}{1 - F_Y(y)}
\end{aligned} \tag{11}$$

where $P_{d\cap}$, $P_{d\cup}$, and $P_{d|}$ are the changes of the simultaneous probability P_{\cap} , the joint probability P_{\cup} , and the conditional probability P_1 after the univariate return period is raised; and x_1 and x_2 are the intensity values of variable X for different return periods, respectively, where $x_2 > x_1$.

3.4.2 Design storm surge and wave criteria for joint return period scenarios

The joint probabilities of storm surge and wave scenarios are hard to be directly employed as reference values for engineering protection standards, since the bivariate joint probability and joint return period is a three-dimensional surface, and the intercepted curve under the specified occurrence probability or return period is a curve, not a scalar. For the combined event of extreme surge height and significant wave height, a series of (x, y) are designed to maximize $P\{X > x, Y > y\}$ under the given joint return period, to obtain the optimal combined design value. Therefore, we explore the design criteria for the combined storm surge and wave scenarios based on the joint return periods RP_{\cup} and simultaneous return periods RP_{\cap} . Under the constraint that the joint return period of surge height and significant wave height is K , the maximum simultaneous bivariate probability is selected as the objective function. This is the case where the bivariate probability is the maximum considering the correlation of two hazard indicators, and the corresponding simultaneous return period is the smallest, which is the most

appropriate case for prevention (Xu et al., 2022). Therefore, the optimal design criteria for storm surge and wave scenarios are estimated using the non-linear programming method (Bazaraa et al., 2006). The formula is expressed as follows:

Constraint condition:

$$\left\{ \begin{array}{l} K = RP_U = \frac{E_L}{P((X > x) \cup (Y > y))} = \frac{E_L}{1 - P(X \leq x, Y \leq y)} = \frac{E_L}{1 - F_{X,Y}(x, y)} \\ x \in (0, 40) \\ y \in (0, 40) \end{array} \right. \quad (12)$$

Objective function:

$$\max \{P_\cap\} = \min \{RP_\cap\} = \min \left\{ \frac{E_L}{P((X > x) \cap (Y > y))} \right\} = \min \left\{ \frac{E_L}{1 - F_X(x) - F_Y(y) + F_{X,Y}(x, y)} \right\} \quad (13)$$

4 Results and discussion

4.1 Optimal marginal function

Since the different densities and locations of the triangular grids in the storm surge and wave models, we use the storm surge triangular grid nodes as the benchmark and the wave node closest to each storm surge node as the wave simulation result based on the nearest neighbor method. Therefore, a dataset of storm surges and waves with the same number and location of nodes is reconstructed, containing 1665 nodes in the study area.

In this paper, based on the reconstructed storm surge and wave simulation results of historical TC events, we calculate each node's annual extreme values of SH and SWH. Firstly, the time series of the bivariate annual maximum value for all nodes are fitted with five marginal functions, including Gumbel, Weibull, gamma, exponential, and generalized extreme value (GEV). Next, the p-value of the K-S test is used to determine whether the hypothesis that the sample obeys a certain theoretical distribution is rejected. Then, we count the number of nodes passing the K-S test for each function and their percentage of all nodes. Finally, the number of nodes and their percentage of each function being selected as optimal is calculated according to the steps for optimal function selection in Section 3.1 (Table 3).

Table 3 Frequency and percentage of five functions passing the K-S test and the optimal function for all nodes of SH and SWH

Marginal	Surge height	Significant wave height
----------	--------------	-------------------------

function	Frequency of K-S test passed	Percentage of K-S test passed (%)	Frequency of optimal function	Percentage of optimal function (%)	Frequency of K-S test passed	Percentage of K-S test passed (%)	Frequency of optimal function	Percentage of optimal function (%)
Gamma	1508	90.57	183	10.99	1464	87.93	159	9.55
Exponential	1567	94.11	216	12.97	1076	64.62	95	5.71
Gumbel (right)	1615	97.00	350	21.02	1629	97.84	149	8.95
Weibull (max)	1469	88.23	416	24.98	300	18.02	494	29.66
GEV	1665	100.00	500	30.04	1657	99.52	768	46.13

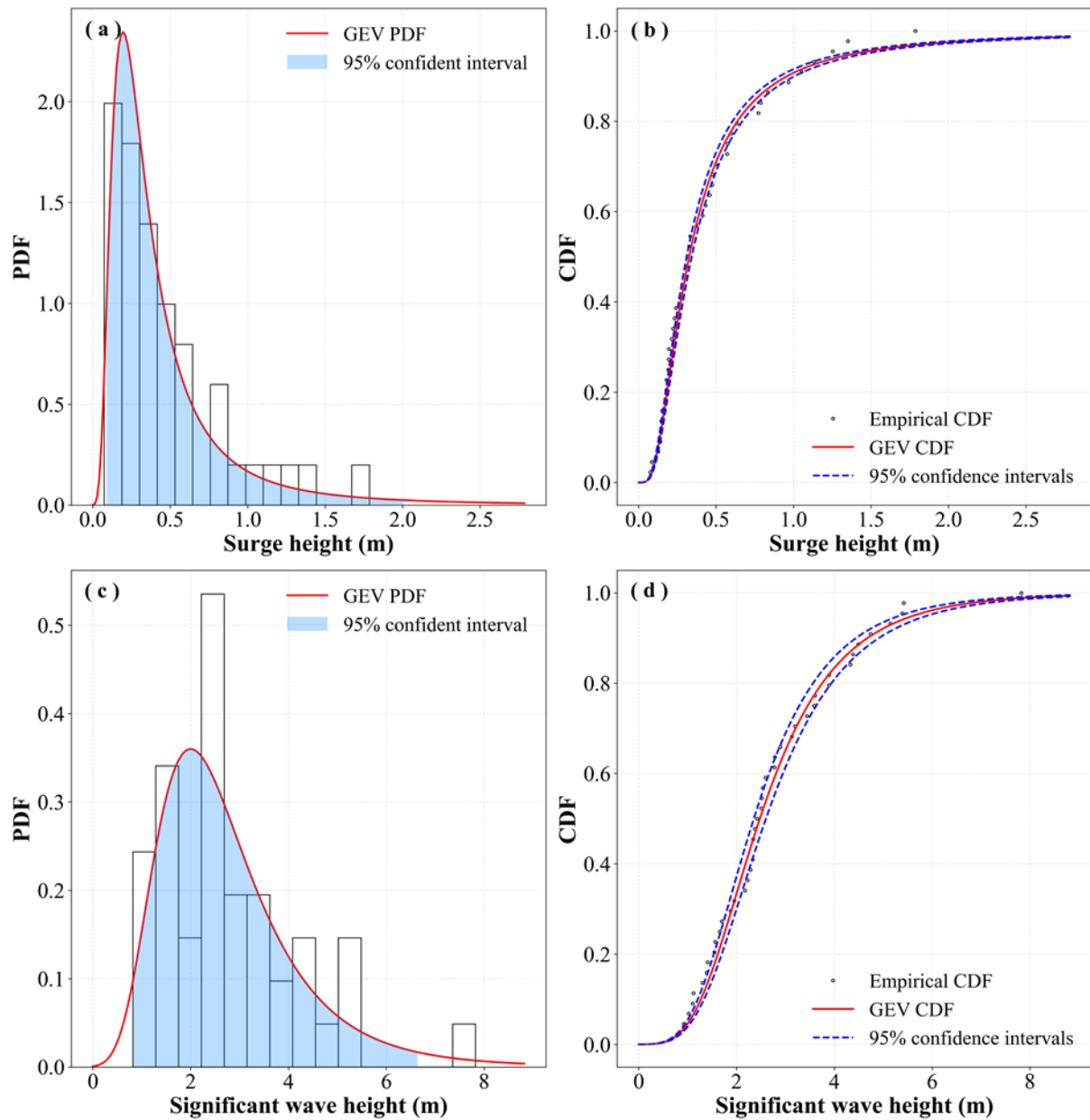


Figure 3: Fitting results of the PDF and CDF of the SH and SWH based on the GEV function (using node (110.5142° E, 20.2768° N) as an example)

210

Based on the statistical results, it is found that for fitting the SH, the K-S test of the GEV function had the highest no-rejection rate of 100%, and the corresponding optimal ratio was 30.04%, so GEV is set as the optimal marginal function in this study. For SWH fitting, the number of nodes with no rejection in the K-S test of the GEV function is 1657, accounting for 99.52%

of the total number of nodes, and the corresponding percentage of preferences is also higher than that of other functions. We
215 apply the GEV function to fit the marginal function of the SH and SWH at all nodes and calculate the PDF, CDF, and RP.
Figure 3 shows an example of the PDF and CDF of the SH and SWH for a given node.

4.2 Distribution of univariate return periods

Based on the univariate return period formula (Eq. 1), the SH and SWH are estimated for six typical return periods of 5a, 10a,
20a, 50a, 100a, and 200a at all nodes. To analyze the distribution characteristics of the univariate return period in this study
220 area, we chose the cubic spline interpolation method to interpolate the intensity values at each node with different return
periods into a raster with a resolution of 1 km (Figure 4 and Figure 5).

As shown in Figure 4, the SH shows a significant increasing trend as it approaches the coastline. The SH along the eastern
coast of the Leizhou Peninsula is higher than that in other regions, mainly influenced by factors such as TC landing location,
landing direction, and pocket-shaped coastal topography. The TCs in the northern hemisphere are counterclockwise rotations
225 affected by the deflecting force. Therefore, northeastern Hainan Island is located on the southern coast of the Qiongzhou Strait,
and the northeast and northwest winds of TCs affecting the region easily cause seawater accumulation, a storm surge-prone
area. The TC wind fields in the east and south of Hainan Island are less favorable to water gain than those in the north. Therefore,
the offshore surge height on Hainan Island shows a distribution pattern of high in the northeast and low in the southeast. As
the return period increases, SH offers varying degrees of growth in each region, and regional differences are more pronounced,
230 with a significant area of development in southeastern Hainan Island, which may be related to the region's location on the edge
of the continental shelf and high variability in seafloor topography.

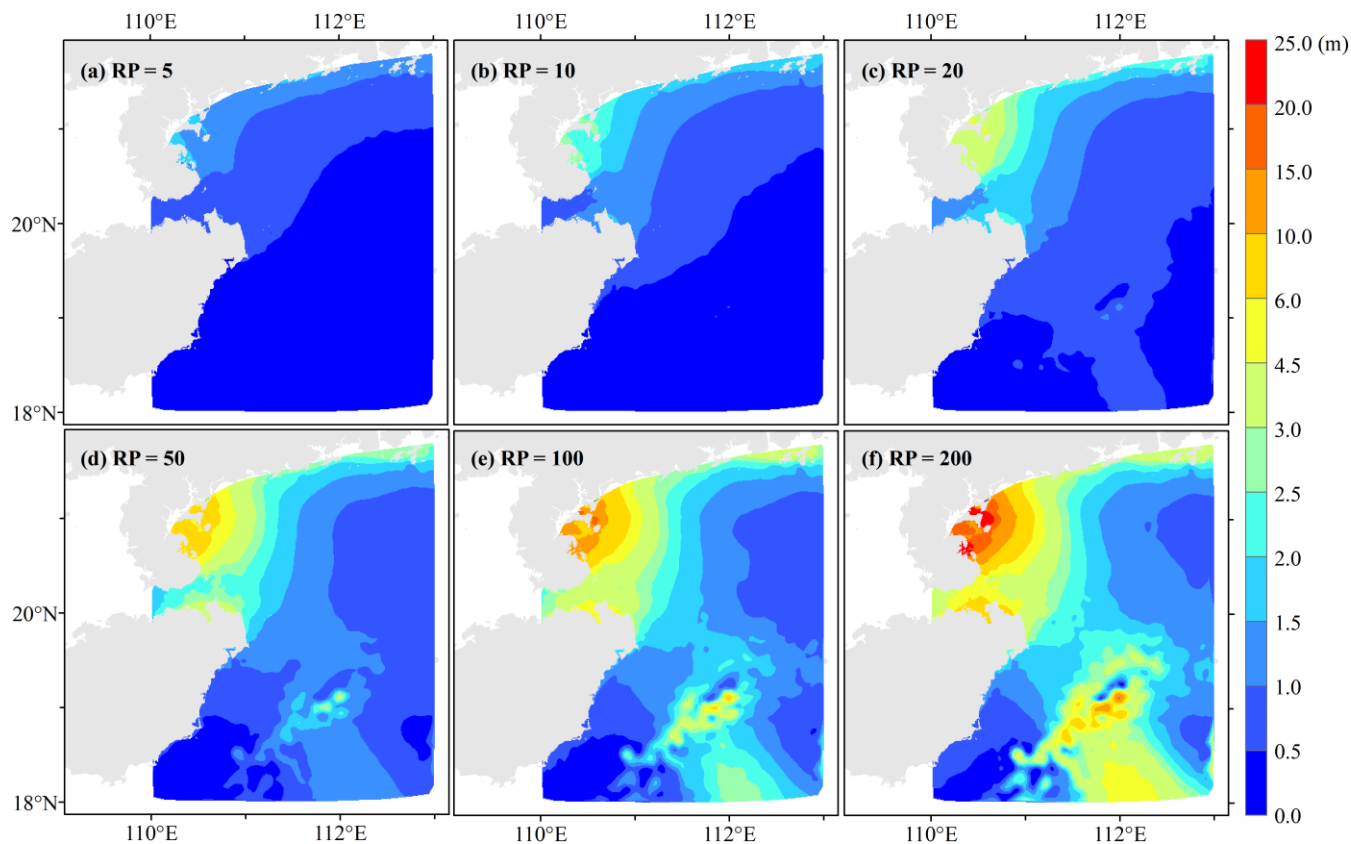


Figure 4: Spatial distribution of surge heights of tropical cyclones for six typical return periods

As shown in Figure 5, the SWH near the shore is generally smaller than that in the open sea, and there is a significant decreasing trend in SWH as it gets closer to the coastline. This finding is mainly attributed to the shallow shore depth, island obstruction, wave breaking, and seabed friction attenuation. Among them, the SWH in the eastern Leizhou Peninsula is lower than that of other seas, which is mainly influenced by the curved depressed coastline and the topography of the shore section. The SWHs are high in the east and south of Hainan Island, where there is a more significant gradient due to the wave-breaking effect and dissipation caused by the region's dramatic change in water depth. The SWH in the north of Hainan Island is low, and the shift from sea to land is relatively slow.

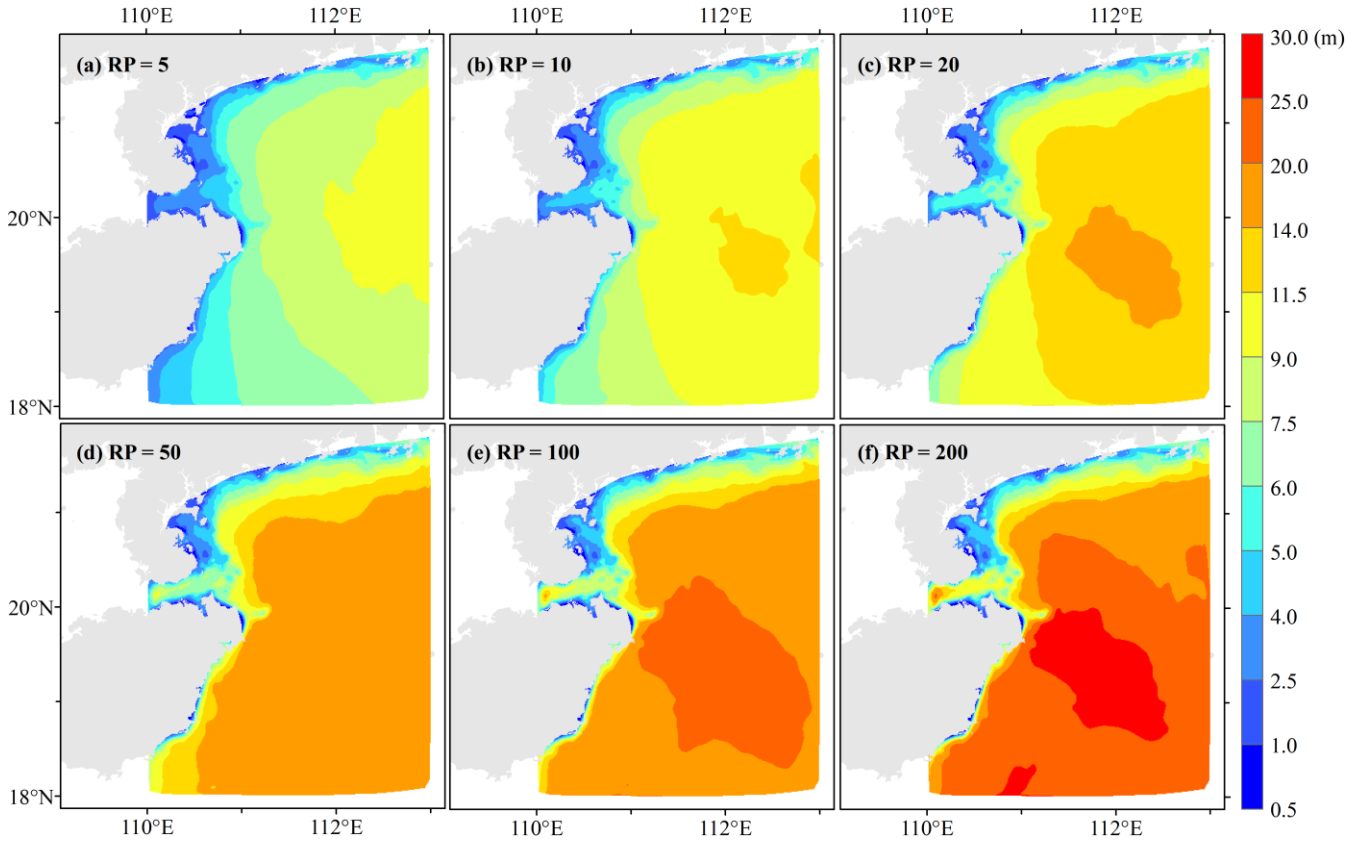


Figure 5: Spatial distribution of significant wave heights of tropical cyclones for six typical return periods

4.3 Optimal copula function

The optimal GEV function is utilized as the marginal function for the TC storm surges and waves, based on which three copula functions are applied to the bivariate joint fitting of 1665 nodes. The function parameters are fitted by the maximum likelihood method, and the K-S test is used to determine whether the hypothesis that the sample obeys a certain functional distribution is rejected. Next, we count the number of nodes that pass the K-S test for the three types of copula functions and their percentage of the total number of nodes (Table 4). The statistical results show that the number of nodes passing the K-S test for the Gumbel copula function is 1603, accounting for 96.28% of all nodes, so it is used as the optimal copula function in this study. The Gumbel copula function is applied to the bivariate joint fitting of SH and SWH for all nodes, and the PDF and CDF are calculated.

Table 4 Frequency and percentage of three copula functions passing the K-S test for all nodes of surge height and significant wave height of tropical cyclones

Copula function	Frequency	Percentage (%)
Clayton	486	29.19
Frank	1398	83.96
Gumbel	1603	96.28

4.4 Distribution of bivariate probabilities and return periods

255 Based on the optimal marginal function and copula function, we calculate RP_{\cap} , RP_{\cup} , and RP_{\perp} of SHs and SWHs. In addition, based on the formula of bivariate probability (Eq. 2 and Eq. 4), P_{\cap} and P_{\cup} of SH and SWH are calculated for all nodes with four typical combinations of return periods of 10a, 20a, 50a, and 100a. To analyze the distribution characteristics, P_{\cap} and P_{\cup} for different combinations of return periods at each node are interpolated into a raster with a resolution of 1 km using the cubic spline interpolation method (Figure 6 and Figure 7).

260 The simultaneous bivariate probability P_{\cap} gradually decreases as the return period of SH or SWH increases (Figure 6). Overall, the closer to the coastline, the higher P_{\cap} . P_{\cap} is greatest when the return period of SH and SWH is 10a, which is higher than 0.05. P_{\cap} is the smallest for SH and SWH of 100a, which is generally lower than 0.009.

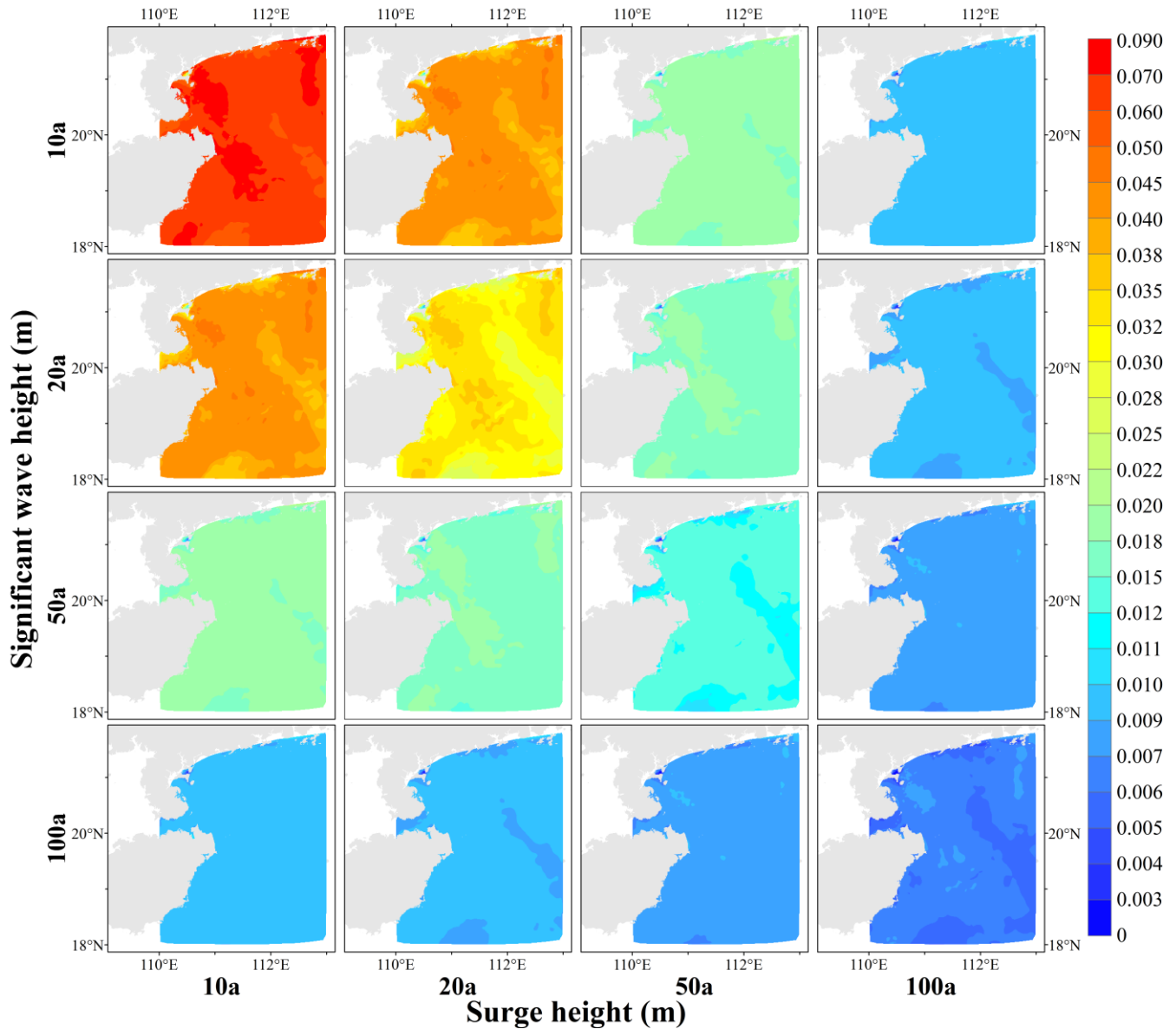


Figure 6: Simultaneous probabilities of combined scenarios with four typical return periods for surge height and significant wave heights of tropical cyclones

265

The joint bivariate probability P_U of SH and SWH is higher than P_{\cap} , and it gradually decreases with an increasing return period of the two hazard indicators (Figure 7). Overall, the closer to the coastline, the higher P_U . P_U is highest when the return period of SH and SWH is 10a, which is greater than 0.13 overall. P_U is smallest when the return period for SH and SWH is 100a, which is less than 0.015. When the return period of SH or SWH is 50a or 100a, the regional variation in P_U are

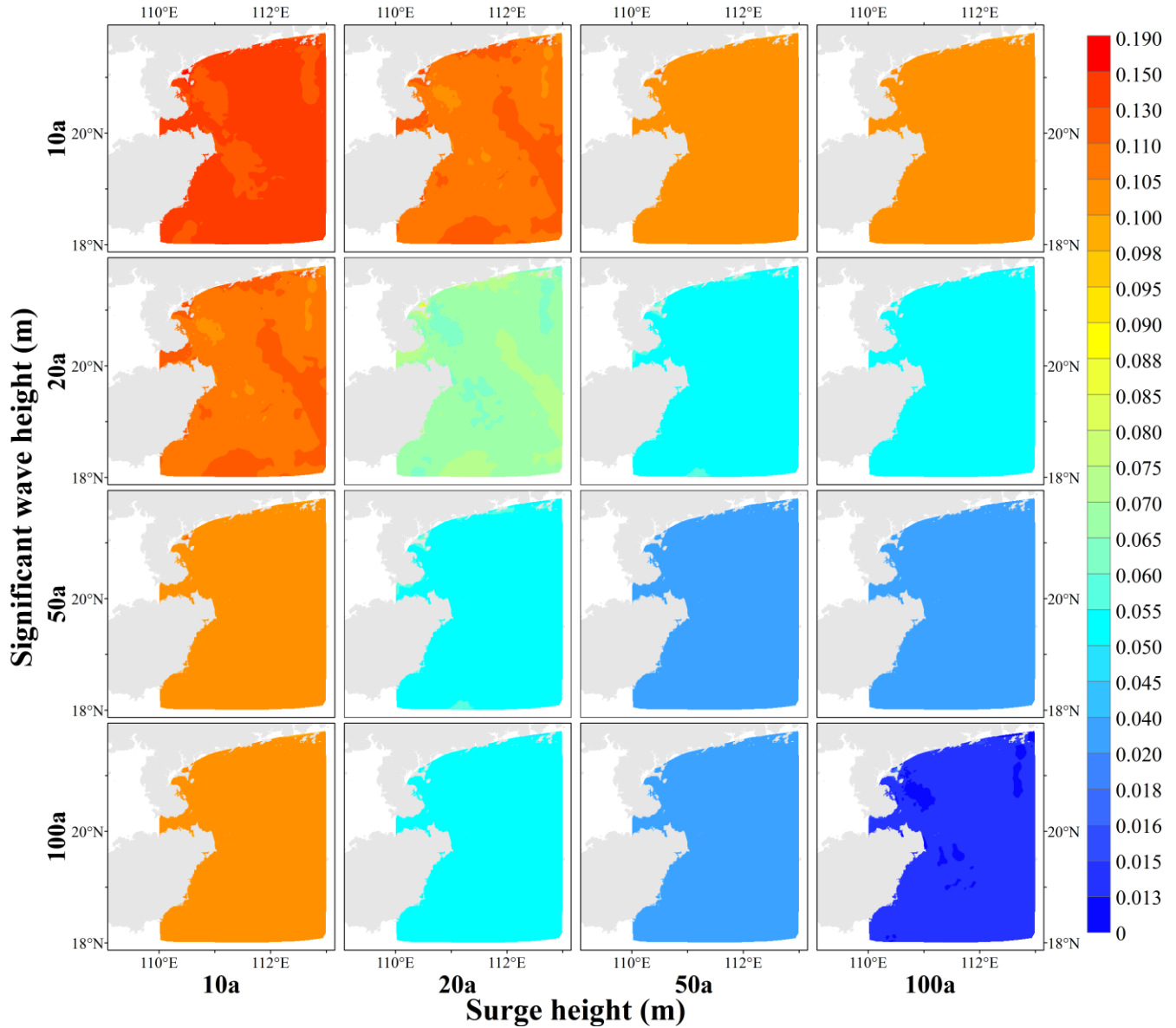


Figure 7: Joint probabilities of combined scenarios with four typical return periods for surge height and significant wave heights of tropical cyclones

Based on the formula of conditional bivariate probability P_i (Eq. 6), we calculate P_i for all nodal univariates with different return periods for the other variable in four return periods, interpolate them into 1 km raster data using cubic spline interpolation. According to the formula, the calculation results are consistent when the positions of the variables are swapped. Therefore,

only P_{\downarrow} for the four return periods of SH in different wave return periods are shown in this paper (Figure 8). When the SWH is a specific return period, P_{\downarrow} gradually decreases as the return period of the SH increases. Under the condition that the return period of SWH is 10a, P_{\downarrow} for SH with a return period of 10a are concentrated between 0.55 and 0.75, and P_{\downarrow} is generally less than 0.08 if the return period for SH is 100a. When the return periods of SWHs and SHs are equivalent, the P_{\downarrow} is concentrated between 0.55 and 0.75.

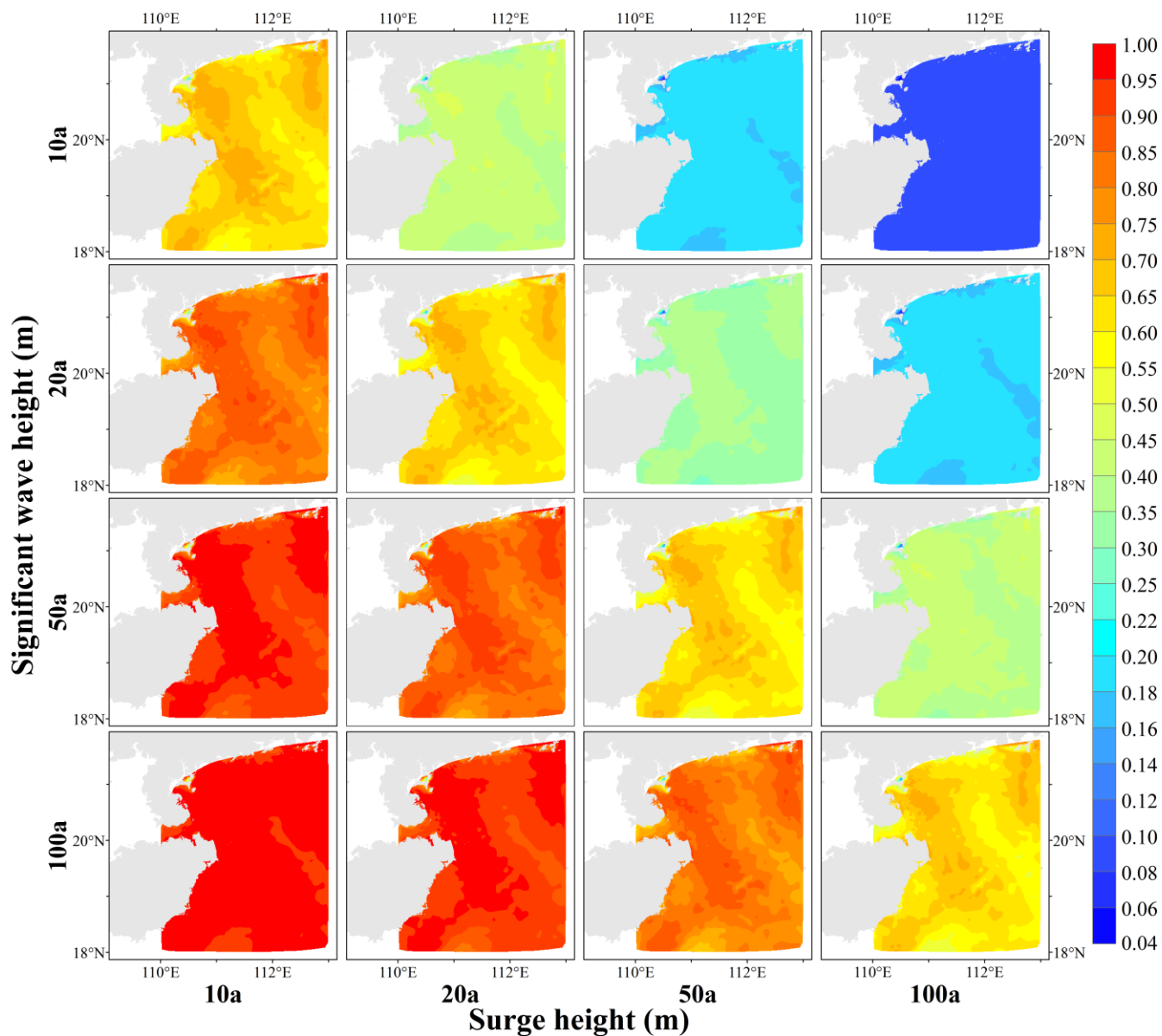


Figure 8: Conditional probabilities of bivariate for different return periods of tropical cyclone significant wave heights

According to the classification criteria of the hazard indicators (Table 2), SH and SWH are divided into five classes. We
285 calculate the combined scenario probability $P_{\&}$ based on Eq. 8 for all nodes with different combinations of SH and SWH for
a total of 25 scenarios and interpolate them into 1 km raster data using the cubic spline interpolation method (Figure 9).
Regarding the vertical variation pattern, when the SH hazard level is determined, as the SWH hazard level increases, the high-
value area of the combined scenario probability gradually moves away from the coastline, and the scope of the nearshore low-
value area gradually expands. This result is consistent with the geographic distribution pattern that the SWH is low in nearshore
290 and high in offshore. In the horizontal variation pattern, when the SWH hazard level is determined, as the SH hazard level
increases, the range of low-value areas for the combined scenario probabilities expand, and the low-value area's left boundary
gradually approaches the coastline. This result is consistent with the geographic distribution of SHs being high nearshore and
low offshore. Overall, the maximum value of the probability for each combined scenario tends to decrease as the hazard level
of SH or SWH increases. The larger SH and SWH are concentrated in the eastern Leizhou Peninsula at a certain distance from
295 the coast, with other areas less likely to occur.

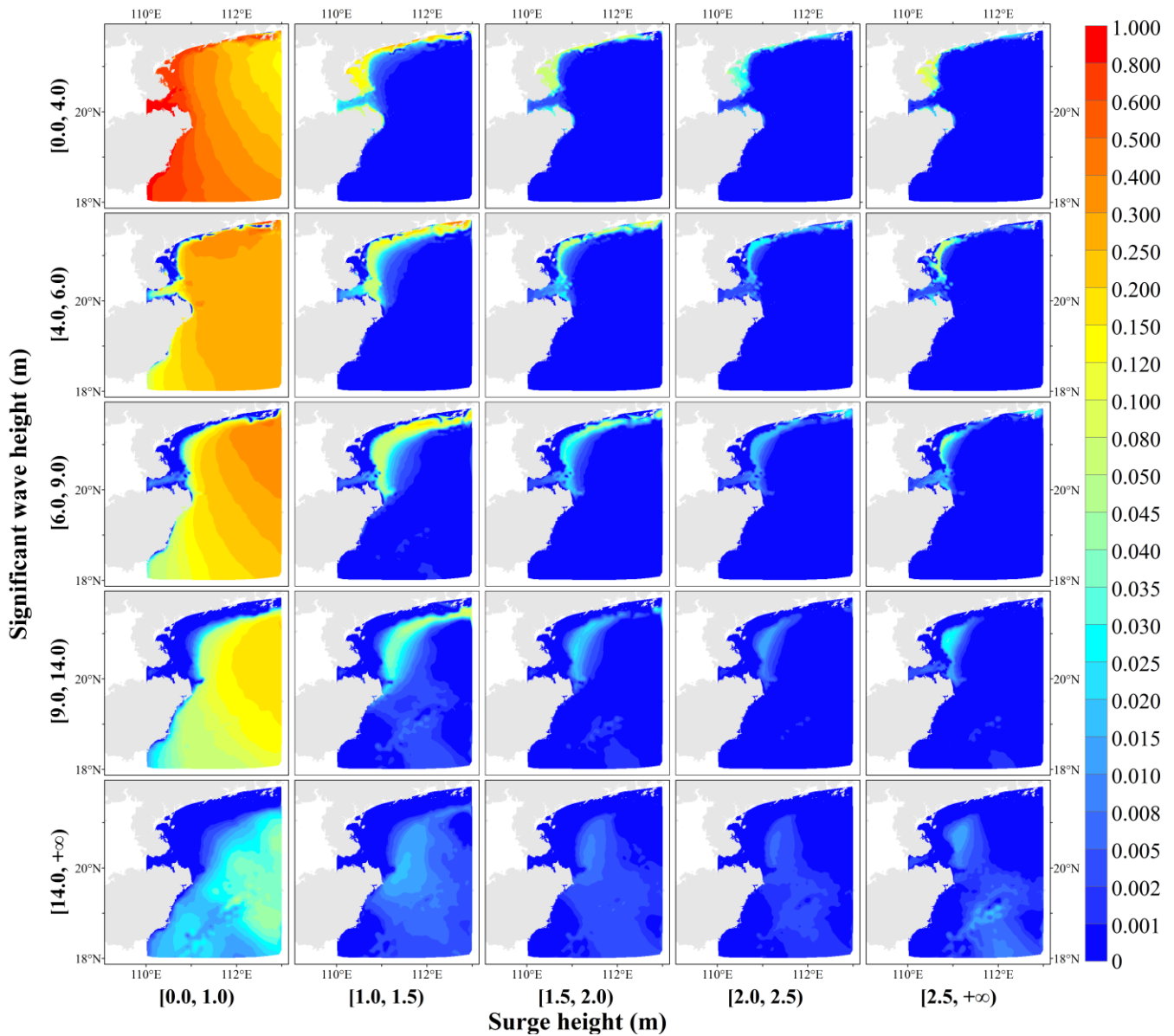


Figure 9: Probabilities of combined scenarios with different levels of surge height and significant wave height for tropical cyclones

Based on the calculated P_{\cap} , P_{\cup} , P_{\setminus} , and $P_{\&}$ with different return periods, Markov chain Monte Carlo (MCMC) and other methods can be further applied to generate random samples for quantitatively assessing TC storm surges and waves. On the other hand, we can explore the effect of varying the intensity values of SH and SWH on the bivariate joint probabilities and apply it to the engineering design criteria.

300

4.5 Design storm surge and wave criteria

In the design of the engineering fortification criteria, if one hazard indicator is dominant, upgrading the return period for the other variable can effectively change bivariate P_{\cap} and P_{\cup} when the conditions for their return period fortification criteria are determined. In this paper, we calculate the change in probability based on Eq. 9, Eq. 10, and Eq. 11 to determine the shift in the probability that remains constant when the positions of the two hazard indicators are switched. Therefore, we calculate the change values in P_{\cap} , P_{\cup} , and P_{\cap} for all nodes when the design return period criterion for a given variable is increased from 5a, 10a, 20a, and 50a to 10a, 20a, 50a, and 100a, respectively. And the data are interpolated into 1 km raster data using the cubic spline interpolation method (Figure 10, Figure 11, and Figure 12).

Figure 10 shows the distribution of the reduction values of bivariate P_{\cap} for the scenario with elevated univariate return period protection criteria. As the return period protection criteria of one variable increase, the decline in P_{\cap} gradually decreases as the return period of the other variable's protection standard increases. Its reduction is concentrated between 0 and 0.035. When the return period protection standard of one variable is fixed, as the protection criteria of another variable are gradually increased, the decline of P_{\cap} rises to a certain level and then tends to decrease. When the return period of one variable is 10a or 20a, the decline in P_{\cap} increases when the protection standard of another variable is raised. If the design criteria increase from 50a to 100a, the change value of P_{\cap} decreases.

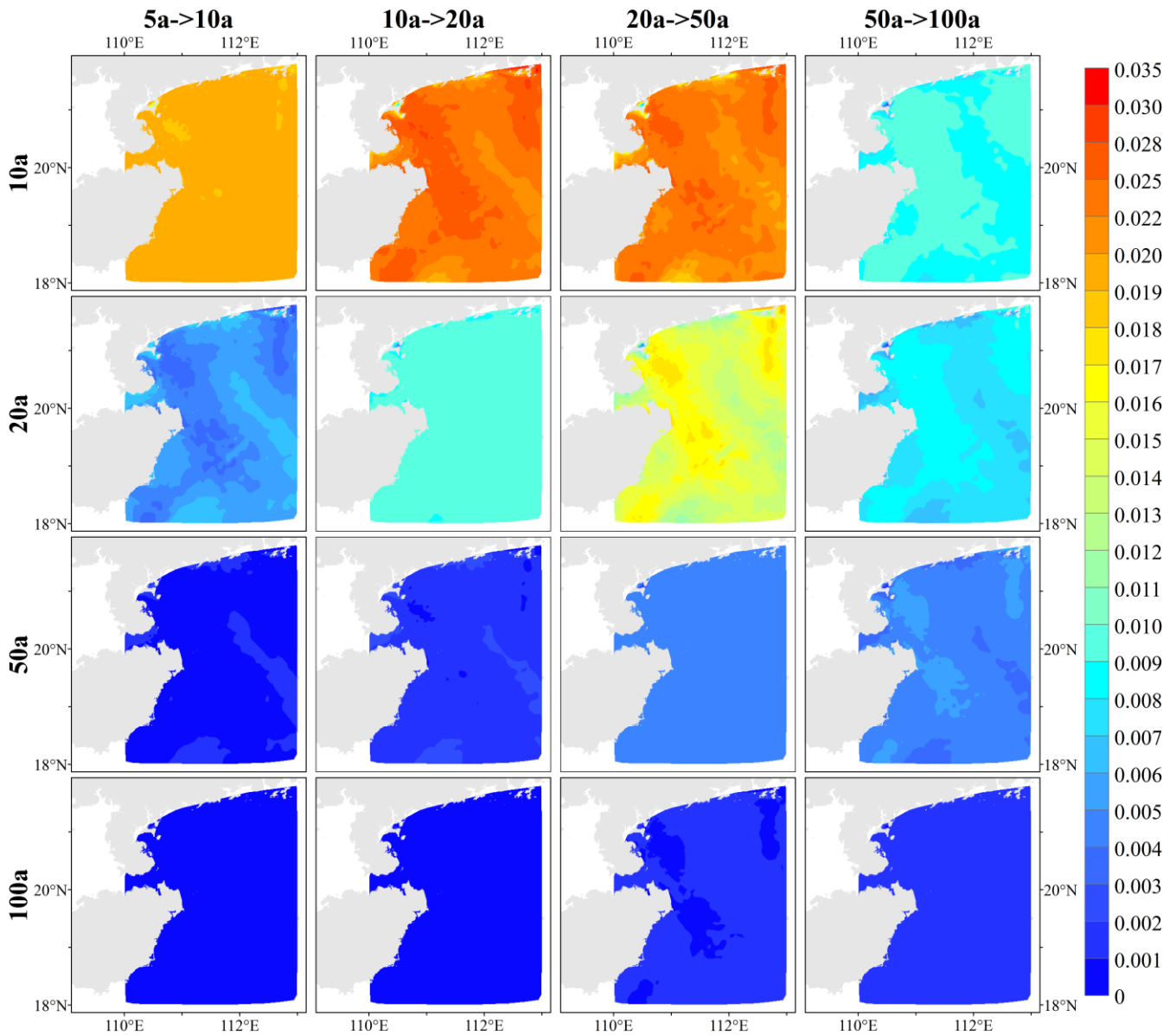


Figure 10: Difference in the simultaneous probability of tropical cyclone surge height and significant wave height for scenarios with elevated return period protection standards

320 Figure 11 shows the distribution of the reduced values for bivariate P_U when the protection criteria for the univariate return period is increased. Among them, P_U decreases more than P_{\cap} , and the reduced value of P_U varies from 0 to 0.105. As the return period protection standard for one variable gradually increases, P_U slowly decreases after the protection criteria for the

other variable increase. When the return period protection criterion for one variable is fixed, the decline in P_U gradually decreases as the design criteria for the other variable are increased.

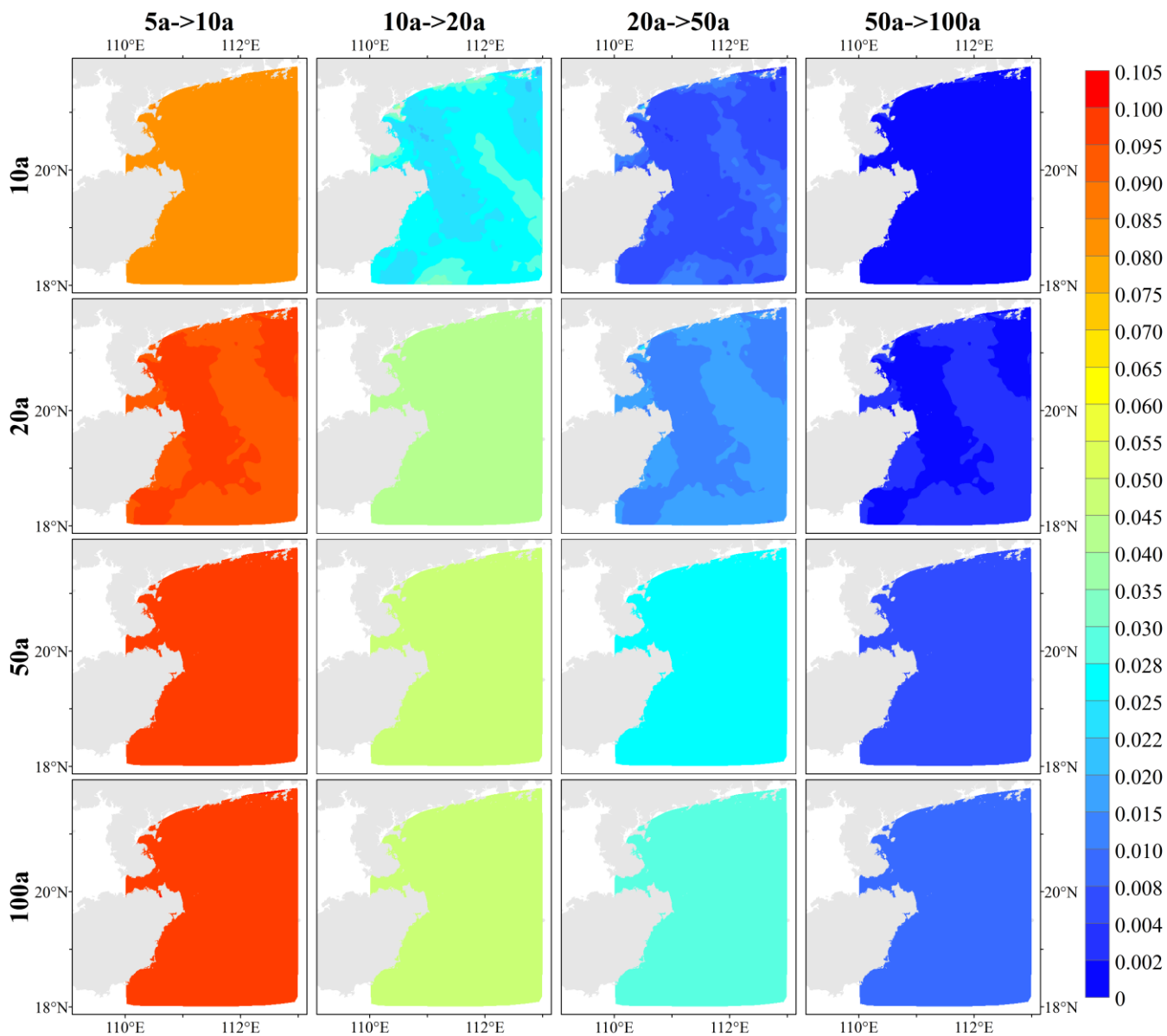


Figure 11: Difference in joint probability of tropical cyclone surge height and significant wave height for scenarios with elevated return period protection standards

Figure 12 shows the distribution of the reduced values of bivariate P_I for the scenario of raising the univariate return period protection criteria. As the return period for one variable increases, there is a decreasing trend in the decrease in P_I after the

330 design criteria for the other variable are raised. P_I has a more significant decrease than P_{\cap} and P_U , and the decreasing value of P_I varies from 0 to 0.45. When the protection level of one variable is fixed and low, the reduction in P_I will tend to decrease after the design criteria of another variable are raised to a certain level. When the protection standard for one variable is 10a or 20a, the decrease in bivariate P_I tends to increase when the design criterion for the other variable's return period is raised, but the decrease in P_I is slightly reduced when the design criterion of the other variable is increased from 50a to 100a.

335 If the protection level of one variable is high, the decrease in P_I after the protection standard of the other variable is raised always tends to increase.

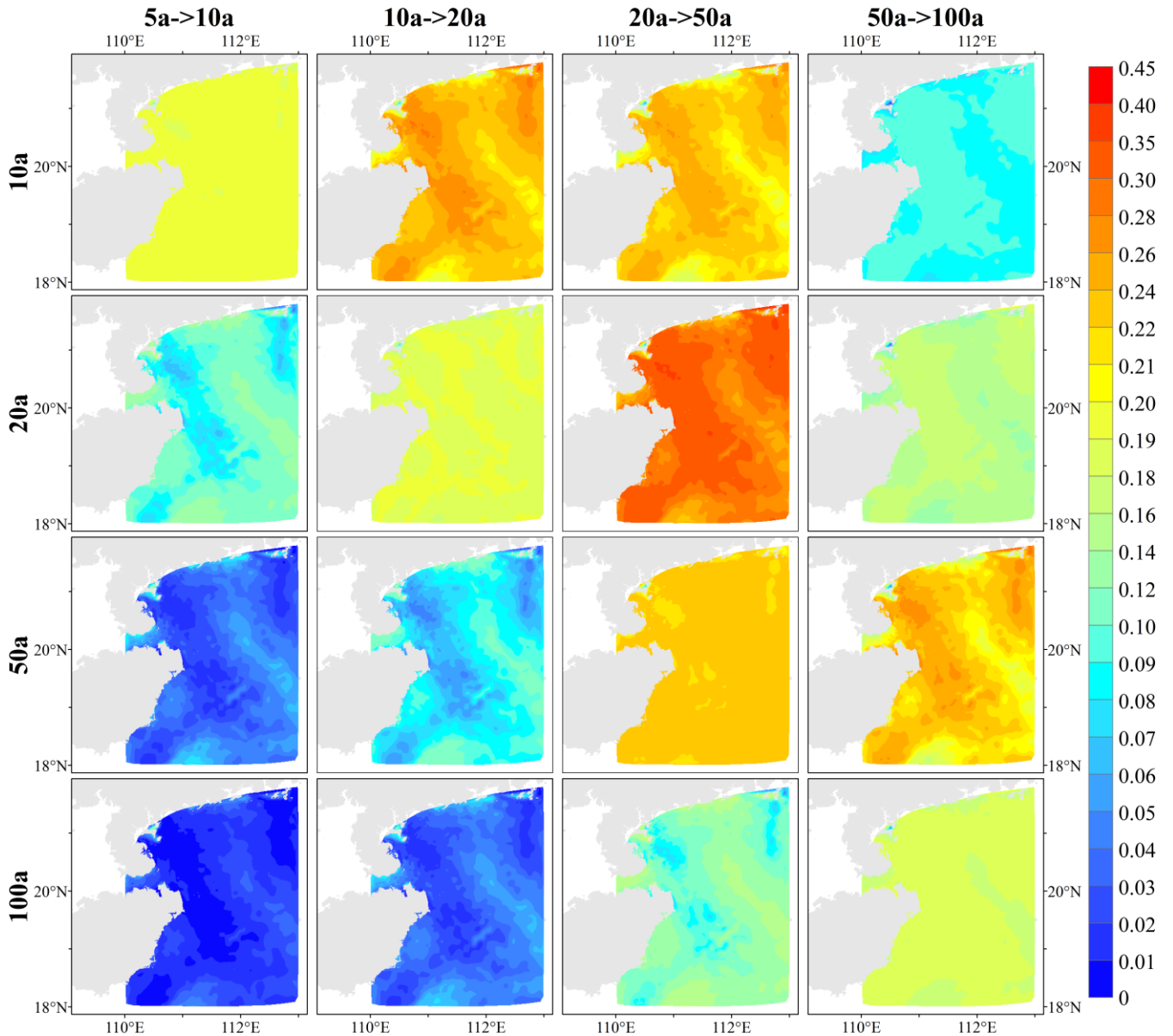


Figure 12: Differences in the conditional probability of tropical cyclone surge height and significant wave height for scenarios with elevated return period protection standards

340 In the engineering design criteria, the appropriate design surge height and significant wave height are set according to the bivariate RP_U and RP_η , the estimation method is shown in Section 3.4.2. In this paper, the design values of SH and SWH for six RP_U for all nodes are calculated based on the above method and interpolated to 1 km raster data by the cubic spline interpolation method (Figure 13 and Figure 14). The design criteria for SH and SWH show an apparent increasing trend as the

return period increases, with the high-value area for SH constantly concentrated east of the Leizhou Peninsula and the high-value area for SWH concentrated in the east of Hainan Island.

When RP_U is 5a, the design criteria of SH are between 1.5 m and 2.5 m in the eastern coastal area of the Leizhou Peninsula and fall below 0.5 m in the southeastern coastal region of Hainan Island. As the return period increases, the design surge height gradually increases, and when RP_U is 200 a, the design surge height in the eastern coastal area of the Leizhou Peninsula is generally higher than 3.0 m. The design surge height in the northeast coastal area of Hainan Island is mainly between 3.0 m and 15.0 m, while that in the southeast coastal region of Hainan Island is between 0.5 m and 2.0 m, which is lower than that in the northeast.

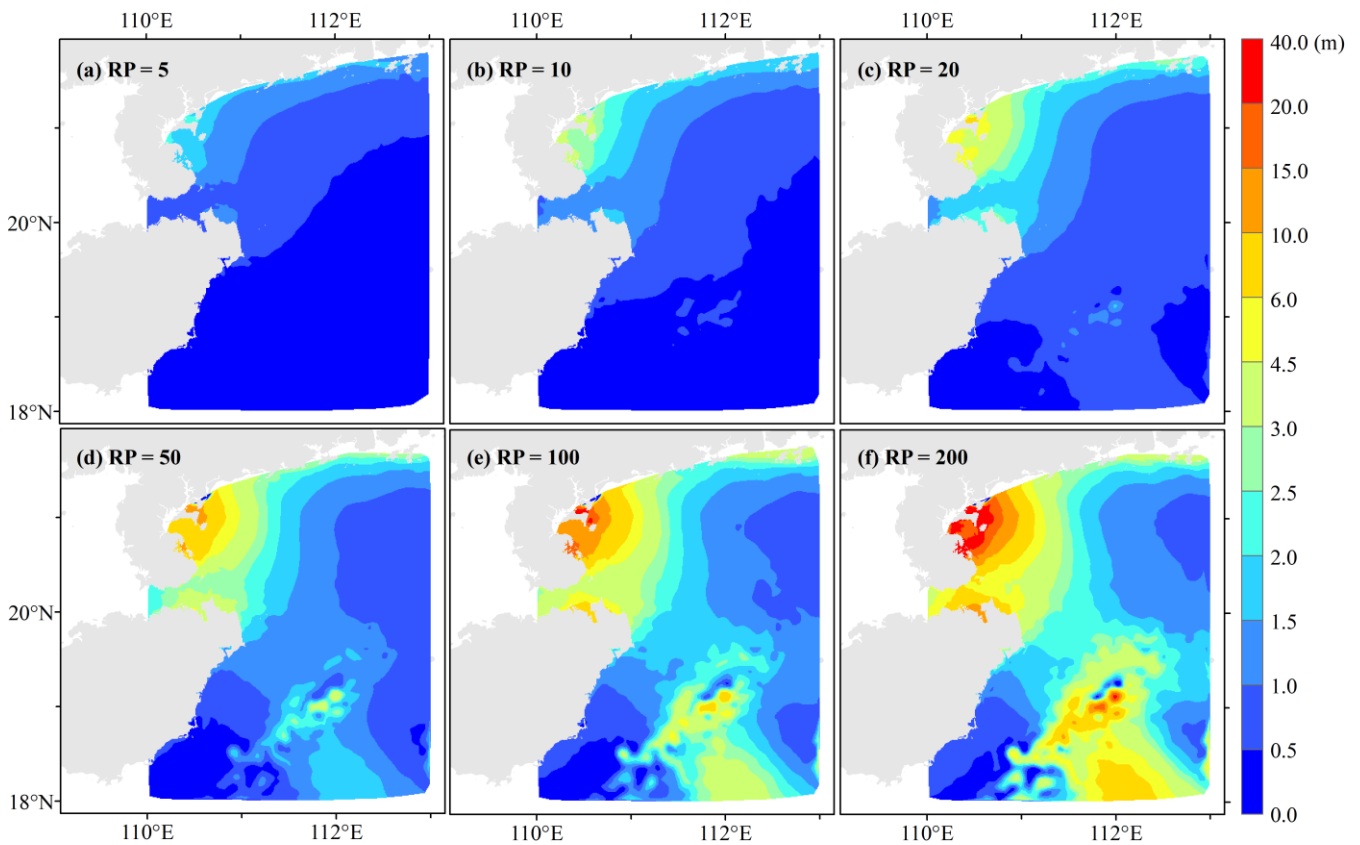
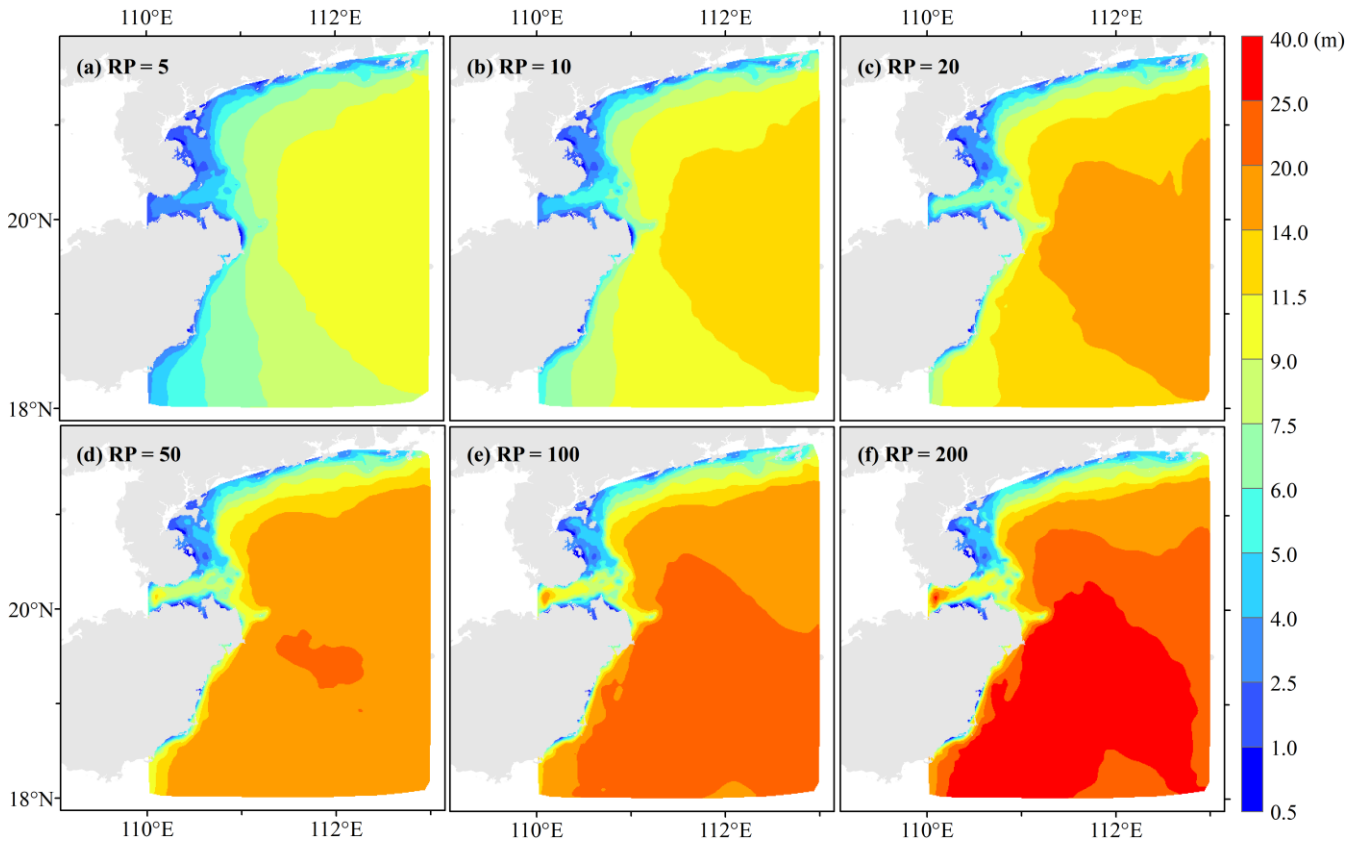


Figure 13: Design surge heights for six typical joint return period scenarios

When RP_U is 5a, the design criteria of SWH in the coastal areas of the Leizhou Peninsula and Hainan Island are less than 2.5 m overall. The further from the coastline, the protection standard gradually increases. As the return period increases, the design

criteria of SWH gradually increase, and the growth is more evident than that of SH. When RP_{\cup} is 200 a, SWH along the coast of the Leizhou Peninsula is generally less than 6.0 m, while the design SWH along the Qiongzhou Strait and southeastern Hainan Island is relatively high.



360 **Figure 14: Design significant wave heights for six typical joint return period scenarios**

5 Conclusions

In this study, we aimed to estimate joint probability analysis on storm surge and waves using Copula functions on a large dataset from a wide area, and determine their respective design standards as scalar values of SWH and SH. Our main conclusions are as follows:

- 365 1) The GEV function is the most suitable for the probability distribution characteristics of the annual extremes of tropical cyclone SH and SWH for all nodes in the study area. The Gumbel copula function is appropriate as a bivariate joint distribution

function for all nodes in the study area.

2) The hazard of a single indicator can be characterized by the univariate intensity values with different return periods, which the optimal marginal function can estimate. Our findings show that the SH exhibits a significant increasing trend closer to the coastline, while SWH is higher farther from the shoreline across different return periods. However, we also observe apparent spatial heterogeneity in the distribution, influenced by factors such as the shoreline shape, coastal and submarine topography, and deflection forces.

3) Bivariate probabilities are utilized in this study to assess the integrated hazard of multiple indicators, including P_{\cap} , P_{\cup} , $P_{|}$, and $P_{\&}$, which effectively compensates for the deficiency of disregarding the correlation among variables in univariate hazard assessment. These four probabilities can visually describe the occurrence probability for different combinations of scenarios; the more significant the probability is, the higher the hazard. Overall, $P_{|}$ is the largest, P_{\cup} is the second largest, and P_{\cap} is the smallest, while $P_{\&}$ is influenced by the classification of single hazard indicators. When one variable is constant, P_{\cap} , P_{\cup} , and $P_{|}$ tend to decrease as the return period of the other variable increases.

4) In actual design criteria, the bivariate P_{\cap} , P_{\cup} , and $P_{|}$ can be reduced by appropriately increasing the design surge height and significant wave height. When the return period protection standard of one variable is fixed, as the design criteria of another variable gradually increase, the decline in P_{\cap} and $P_{|}$ rises to a certain level and then tends to decrease, but the decline in P_{\cup} gradually decreases. Therefore, the development of appropriate design surge heights and significant wave heights can be effective in reducing hazard impacts, which allows coastal areas to cope with a high bivariate probability. To obtain the specific scaler values of the two hazards as design criteria, in this study, the method for estimating the minimum return periods of SH and SWH was implemented, given their estimated joint probability distribution as a constraint.

Although this study provides helpful insights into joint probability analysis of storm surges and waves using Copula functions, there are several limitations that need to be addressed in future research. One limitation is the absence of water level rise caused by storm surges in the numerical modeling of waves, which may introduce errors in the simulation of SWHs in intermediate and shallow water. In addition, exploring the contribution of other indicators, such as long-term sea level rise as environmental hazards, can further improve the accuracy of risk assessment.

Author contributions. FWH and ZHX conceived the research framework and developed the methodology. ZHX was responsible for the code compilation, data analysis, graphic visualization, and first draft writing. FWH managed the implementation of research activities and revised the manuscript. CM participated in the data collection of this study. All authors discussed the results and contributed to the final version of the paper.

395 **Competing interests.** The authors declare that they have no conflict of interest.

Acknowledgments. This work was mainly supported by the National Key Research and Development Program of China (grant nos. 2017YFA0604903 and 2018YFC1508803) and the Key Special Project for Introduced Talents Team of Southern Marine Science and Engineering Guangdong Laboratory (Guangzhou) (grant no. GML2019ZD0601). We are grateful to Xing Liu of the Ocean University of China for providing the simulation data of storm surges and waves for historical tropical cyclone
400 events.

Financial support. This research has been supported by the National Key Research and Development Program of China (grant nos. 2017YFA0604903 and 2018YFC1508803), and the Key Special Project for Introduced Talents Team of Southern Marine Science and Engineering Guangdong Laboratory (Guangzhou) (grant no. GML2019ZD0601).

References

- 405 Bazaraa, M. S., Sherali, H. D., and Shetty, C. M.: Nonlinear programming: Theory and algorithms, Third Edit., John Wiley & Sons, Ltd, Hoboken, New Jersey, 872 pp., <https://doi.org/https://doi.org/10.1002/0471787779>, 2006.
- Bilskie1, M. V., Hagen, S. C., Medeiros, S. C., Cox, A. T., Salisbury, M., and Coggin, D.: Data and numerical analysis of astronomic tides, wind-waves, and hurricane storm surge along the northern Gulf of Mexico, *J. Geophys. Res. Ocean.*, 121, 3625–3658, <https://doi.org/10.1002/2015JC011400>, 2016.
- 410 Bomers, A., Schielen, R. M. J., and Hulscher, S. J. M. H.: Consequences of dike breaches and dike overflow in a bifurcating river system, *Nat. Hazards*, 97, 309–334, <https://doi.org/10.1007/s11069-019-03643-y>, 2019.
- Brown, J. M.: A case study of combined wave and water levels under storm conditions using WAM and SWAN in a shallow water application, *Ocean Model.*, 35, 215–229, <https://doi.org/10.1016/j.ocemod.2010.07.009>, 2010.
- Chen, L. and Guo, S.: Copulas and its application in hydrology and water resources, First Edit., Springer Singapore, Singapore, 290 pp., <https://doi.org/10.1007/978-981-13-0574-0>, 2019.
- 415 Chen, Y. and Yu, X.: Sensitivity of storm wave modeling to wind stress evaluation methods, *J. Adv. Model. Earth Syst.*, 9, 893–907, <https://doi.org/10.1002/2016MS000850>, 2017.

- Chen, Y., Li, J., Pan, S., Gan, M., Pan, Y., Xie, D., and Clee, S.: Joint probability analysis of extreme wave heights and surges along China's coasts, *Ocean Eng.*, 177, 97–107, <https://doi.org/10.1016/j.oceaneng.2018.12.010>, 2019.
- 420 Corbella, S. and Stretch, D. D.: Simulating a multivariate sea storm using Archimedean copulas, *Coast. Eng.*, 76, 68–78, <https://doi.org/10.1016/j.coastaleng.2013.01.011>, 2013.
- Galiatsatou, P. and Prinos, P.: Joint probability analysis of extreme wave heights and storm surges in the Aegean Sea in a changing climate, *E3S Web Conf.*, 7, 1–12, <https://doi.org/10.1051/e3sconf/20160702002>, 2016.
- Hsu, C. H., Olivera, F., and Irish, J. L.: A hurricane surge risk assessment framework using the joint probability method and surge response functions, *Nat. Hazards*, 91, S7–S28, <https://doi.org/10.1007/s11069-017-3108-8>, 2018.
- 425 Huang, Y., Weisberg, R. H., Zheng, L., and Zijlema, M.: Gulf of Mexico hurricane wave simulations using SWAN: Bulk formula-based drag coefficient sensitivity for Hurricane Ike, *J. Geophys. Res. Ocean.*, 118, 3916–3938, <https://doi.org/10.1002/jgrc.20283>, 2013.
- Hughes, S. A. and Nadal, N. C.: Laboratory study of combined wave overtopping and storm surge overflow of a levee, *Coast. Eng.*, 56, 244–259, <https://doi.org/10.1016/j.coastaleng.2008.09.005>, 2009.
- 430 Jang, J. H. and Chang, T. H.: Flood risk estimation under the compound influence of rainfall and tide, *J. Hydrol.*, 606, 127446, <https://doi.org/10.1016/j.jhydrol.2022.127446>, 2022.
- Kimf, K. O., Yuk, J., Leen, H. S., and Choi, B. H.: Typhoon Morakot induced waves and surges with an integrally coupled tide-surge-wave finite element model, *J. Coast. Res.*, 2, 1122–1126, <https://doi.org/10.2112/S175-225.1>, 2016.
- 435 Lee, D. Y. and Jun, K. C.: Estimation of design wave height for the waters around the Korean Peninsula, *Ocean Sci. J.*, 41, 245–254, <https://doi.org/10.1007/BF03020628>, 2006.
- Lee, T., Modarres, R., and Ouarda, T. B. M. J.: Data-based analysis of bivariate copula tail dependence for drought duration and severity, *Hydrol. Process.*, 27, 1454–1463, <https://doi.org/10.1002/hyp.9233>, 2013.
- 440 Li, J., Fang, W., Zhang, X., Cao, S., Yang, X., Liu, X., and Sun, J.: Similar tropical cyclone retrieval method for rapid potential storm surge and wave disaster loss assessment based on multiple hazard indicators, *Mar. Sci.*, 40, 49–60, <https://doi.org/10.11759/hydx20151104001>, 2016.
- Li, L., Pan, Y., Amini, F., and Kuang, C.: Full scale study of combined wave and surge overtopping of a levee with RCC strengthening system, *Ocean Eng.*, 54, 70–86, <https://doi.org/10.1016/j.oceaneng.2012.07.021>, 2012.
- 445 Lin, N., Emanuel, K. A., Smith, J. A., and Vanmarcke, E.: Risk assessment of hurricane storm surge for New York City, *J. Geophys. Res. Atmos.*, 115, 1–11, <https://doi.org/10.1029/2009JD013630>, 2010.
- Liu, X., Jiang, W., Yang, B., and Baugh, J.: Numerical study on factors influencing typhoon-induced storm surge distribution in Zhanjiang Harbor, *Estuar. Coast. Shelf Sci.*, 215, 39–51, <https://doi.org/10.1016/j.ecss.2018.09.019>, 2018.
- 450 Lu, X., Yu, H., Ying, M., Zhao, B., Zhang, S., Lin, L., Bai, L., and Wan, R.: Western North Pacific Tropical Cyclone Database Created by the China Meteorological Administration, *Adv. Atmos. Sci.*, 38, 690–699, <https://doi.org/10.1007/s00376-020-0211-7>, 2021.
- Marcos, M., Rohmer, J., Vousedoukas, M. I., Mentaschi, L., Le Cozannet, G., and Amores, A.: Increased extreme coastal water levels due to the combined action of storm surges and wind waves, *Geophys. Res. Lett.*, 46, 4356–4364, <https://doi.org/10.1029/2019GL082599>, 2019.
- MNR: Technical directives for risk assessment and zoning of marine disaster--Part 1: Storm surge, 2019.

- 455 MNR: Technical directives for risk assessment and zoning of marine disaster--Part 2: Wave, Beijing, 1–30 pp., 2021.
- Morellato, D. and Benoit, M.: Constitution of a numerical wave data-base along the French Mediterranean coasts through hindcast simulations over 1979–2008, *Chart*, 1–8, <https://doi.org/10.13140/2.1.1794.3049>, 2010.
- Muraleedharan, G., Rao, A. D., Kurup, P. G., Nair, N. U., and Sinha, M.: Modified Weibull distribution for maximum and significant wave height simulation and prediction, *Coast. Eng.*, 54, 630–638, <https://doi.org/10.1016/j.coastaleng.2007.05.001>,
460 2007.
- Nelsen, R. B.: An introduction to copulas, Second Edi., Springer Science+Business Media, New York, 1–656 pp., 2006.
- Niedoroda, A. W., Resio, D. T., Toro, G. R., Divoky, D., Das, H. S., and Reed, C. W.: Analysis of the coastal Mississippi storm surge hazard, *Ocean Eng.*, 37, 82–90, <https://doi.org/10.1016/j.oceaneng.2009.08.019>, 2010.
- Pan, Y., Li, L., Amini, F., and Kuang, C.: Full-scale HPTRM-strengthened levee testing under combined wave and surge overtopping conditions: Overtopping hydraulics, shear stress, and erosion analysis, *J. Coast. Res.*, 29, 182–200,
465 <https://doi.org/10.2112/JCOASTRES-D-12-00010.1>, 2013.
- Pan, Y., Zhang, Z., Yuan, S., Zhou, Z., and Chen, Y.: An overview of research on combined wave and surge overtopping on levees, *Adv. Sci. Technol. Water Resour.*, 39, 90–94, <https://doi.org/10.3880/j.issn.1006-7647.2019.01.015>, 2019.
- Papadimitriou, A. G., Chondros, M. K., Metallinos, A. S., Memos, C. D., and Tsoukala, V. K.: Simulating wave transmission in the lee of a breakwater in spectral models due to overtopping, *Appl. Math. Model.*, 88, 743–757,
470 <https://doi.org/10.1016/j.apm.2020.06.061>, 2020.
- Perk, L., van Rijn, L., Koudstaal, K., and Fordeyn, J.: A rational method for the design of sand dike/dune systems at sheltered sites; Wadden Sea Coast of Texel, the Netherlands, *J. Mar. Sci. Eng.*, 7, 1–25, <https://doi.org/10.3390/jmse7090324>, 2019.
- Petroliaqkis, T. I., Voukouvalas, E., Disperati, J., and Bidlot, J.: Joint probabilities of storm surge, significant wave height and river discharge components of coastal flooding events. Utilising statistical dependence methodologies and techniques, Publications Office of the European Union, Luxembourg, 79 pp., <https://doi.org/10.2788/677778>, 2016.
- Rao, X., Li, L., Amini, F., and Tang, H.: Numerical study of combined wave and surge overtopping over RCC strengthened levee systems using the smoothed particle hydrodynamics method, *Ocean Eng.*, 54, 101–109,
475 <https://doi.org/10.1016/j.oceaneng.2012.06.024>, 2012.
- Serinaldi, F.: Dismissing return periods!, *Stoch. Environ. Res. Risk Assess.*, 29, 1179–1189, <https://doi.org/10.1007/s00477-014-0916-1>, 2015.
- Shi, X., Han, Z., Fang, J., Tan, J., Guo, Z., and Sun, Z.: Assessment and zonation of storm surge hazards in the coastal areas of China, *Nat. Hazards*, 100, 39–48, <https://doi.org/10.1007/s11069-019-03793-z>, 2020.
- Sklar, A.: Random variables, joint distribution functions, and copulas, *Kybernetika*, 9, 449–460, 1973.
- 485 Teena, N. V., Sanil Kumar, V., Sudheesh, K., and Sajeew, R.: Statistical analysis on extreme wave height, *Nat. Hazards*, 64, 223–236, <https://doi.org/10.1007/s11069-012-0229-y>, 2012.
- Trepanier, J. C., Needham, H. F., Elsner, J. B., and Jagger, T. H.: Combining surge and wind risk from hurricanes using a copula model: An example from Galveston, Texas, *Prof. Geogr.*, 67, 52–61, <https://doi.org/10.1080/00330124.2013.866437>,
480 2015.
- 490 Wahl, T., Mudersbach, C., and Jensen, J.: Assessing the hydrodynamic boundary conditions for risk analyses in coastal areas: A multivariate statistical approach based on Copula functions, *Nat. Hazards Earth Syst. Sci.*, 12, 495–510,

<https://doi.org/10.5194/nhess-12-495-2012>, 2012.

Wahl, T., Jain, S., Bender, J., Meyers, S. D., and Luther, M. E.: Increasing risk of compound flooding from storm surge and rainfall for major US cities, *Nat. Clim. Chang.*, 5, 1093–1097, <https://doi.org/10.1038/nclimate2736>, 2015.

495 Xie, D. mei, Zou, Q. ping, and Cannon, J. W.: Application of SWAN+ADCIRC to tide-surge and wave simulation in Gulf of Maine during Patriot’s Day storm, *Water Sci. Eng.*, 9, 33–41, <https://doi.org/10.1016/j.wse.2016.02.003>, 2016.

Xu, H., Tan, J., Li, M., and Wang, J.: Compound flood risk of rainfall and storm surge in coastal cities as assessed by copula formal, *J. Nat. Disasters*, 31, 40–48, <https://doi.org/10.13577/j.jnd.2022.0104>, 2022.

500 Zhang, B. and Wang, S.: Probabilistic characterization of extreme storm surges induced by tropical cyclones, *J. Geophys. Res. Atmos.*, 126, 1–22, <https://doi.org/10.1029/2020JD033557>, 2021.